Contents lists available at ScienceDirect

Journal of Hydrology

Research papers

Rapid surface water expansion due to increasing artificial reservoirs and aquaculture ponds in North China Plain

Yan Zhou [a,b,c], Jinwei Dong [c,*], Yaoping Cui [a,b], Sha Zhou [d], Zhichao Li [c], Xinxin Wang [e,f], Xiangzheng Deng [c], Zhenhua Zou [g], Xiangming Xiao [f,*]

[a] *Key Laboratory of Geospatial Technology for the Middle and Lower Yellow River Regions (Henan University), Ministry of Education, Kaifeng 475004, China*
[b] *College of Geography and Environmental Science, Henan University, Kaifeng 475004, China*
[c] *Key Laboratory of Land Surface Pattern and Simulation, Institute of Geographic Sciences and Natural Resources Research, Chinese Academy of Sciences, Beijing 100101, China*
[d] *Faculty of Geographical Sciences, Beijing Normal University, Beijing 100081, China*
[e] *Ministry of Education Key Laboratory for Biodiversity Science and Ecological Engineering, National Observations and Research Station for Wetland Ecosystems of the Yangtze Estuary, Institute of Biodiversity Science and Institute of Eco-Chongming, School of Life Sciences, Fudan University, Shanghai 200438, China*
[f] *Department of Microbiology and Plant Biology, University of Oklahoma, Norman, OK 73019, USA*
[g] *Department of Geographical Sciences, University of Maryland, College Park, MD 20742, USA*

A R T I C L E   I N F O

A B S T R A C T

Water shortage has severely threatened the North China Plain (NCP), a typical grain bowl and highly populated and urbanized area in China. As surface water body area (SWA) is a critical variable for measuring regional water resources, understanding its changes and driving mechanisms is important for sustainable water management. Here, we examine the interannual variations and trends of SWA in the NCP during 1987–2020 by using all the available Landsat imagery, the water indices- and threshold-based water mapping algorithm, and cloud computing platform Google Earth Engine (GEE). The results show that SWA of the NCP significantly ($p < 0.05$) expanded by 68.0% (from 4740.0 km^2 in 1987 to 7963.7 km^2 in 2020) at a rate of 101.9 km^2/yr. The most remarkable expansion of SWA happened in Shandong Province (75.0 km^2/yr), which is an increasingly important aquaculture production region. We find that the increasing artificial reservoirs/lakes due to the implementation of water projects, together with aquaculture development, are the main drivers for the expansion of SWA in the NCP. The expansion of SWA caused a significant increase in water evaporation (0.09 km^3/yr) in the NCP as the shallow nature of these artificial reservoirs/lakes and aquaculture ponds could lead to excess evaporation because of the frequent heating and cooling cycles due to their limited abilities to store energy. Similarly, Shandong Province experienced the most rapid increase in water evaporation (0.03 km^3/yr), which could accelerate the loss of water storage at a rate of 8.4–14.4 mm/yr in the regions covered by surface water bodies. Continuous temperature rise (0.02–0.06 °C/yr) in the future, as predicted by the climate models (CMIP5) under the two Representative Concentration Pathway (RCP) scenarios of medium (RCP 4.5) and high (RCP 8.5) greenhouse gas emission, could further increase water evaporation, which may add more pressure to regional water shortage. This study warns that, despite an observed significant SWA expansion, water shortage remains a major concern in the NCP.

1. Introduction

Water shortage is one of the most significant factors limiting sustainable development in the North China Plain (NCP), one of the most important agricultural production regions and densely populated areas in China (Guo and Shen 2015; Liu et al. 2001; Qin et al. 2013). Surface water bodies, including lakes, reservoirs, ponds, rivers, and streams, are critically important water resources for industrial and agricultural production, as well as biodiversity conservation in riparian and wetland ecosystems (Huang et al. 2018; Vörösmarty et al., 2010; Xie et al. 2017; Zou et al. 2018). Surface water bodies are dynamic owing to different natural and anthropogenic drivers (Hall et al. 2014). The changes in

---

* Corresponding authors.
E-mail addresses: dongjw@igsnrr.ac.cn (J. Dong), xiangming.xiao@ou.edu (X. Xiao).

surface water bodies could affect water evaporation and, subsequently, regional water resources (Zhan et al. 2019). The spatial distribution, temporal dynamics, and long-term trends of surface water bodies can provide valuable information for water-resource planning and management in coping with climate change and human disturbance (Zou et al. 2018). However, the information about the dynamics and long-term trends of surface water bodies in the NCP to the present remains underexplored. In addition, the studies about the effects of the dynamics of surface water bodies on total water storage in the NCP are still limited, which hinders our capability to achieve sustainable management of water resources.

The rapid development of remote sensing technology in recent decades provides an effective way to monitor the dynamics of surface water bodies (Huang et al. 2018), especially in remote and inaccessible mountainous regions (Song et al. 2013; Zhang et al. 2011). Compared to traditional *in situ* measurements, satellites could provide observations with high frequency for continuous monitoring of surface water bodies over a large region. A few data products on the spatial distributions of surface water bodies with various spatial and temporal resolutions have been released based on satellite imagery, such as Global Water Body data (GLOWABO) at 30 m resolution for the year 2000 (Verpoorter et al. 2014) and Global 3 arc-second Water Body Map (G3WBM) for 2010 (Yamazaki et al. 2015). However, limited by data availability and the processing capacity of platforms, these single-period static maps cannot precisely depict the dynamic processes (e.g., interannual variations) of changes in surface water bodies. Using MODIS imagery, Ji et al. (2018) generated the Daily Global Surface Water Change Database at 500-m resolution for 2001–2016. However, the spatial resolution of the data is too coarse to identify small inland water bodies. In 2016, the Joint Research Centre (JRC) (Pekel et al. 2016) released the yearly global water body maps at 30 m spatial resolution from 1984 to 2015. However, the data missed some surface water bodies in China before the year 2000. Though the entire Landsat 5/7/8 top-of-atmosphere (TOA) reflectance data were used to generate the JRC data set (Pekel et al. 2016), the data archiving of Landsat images is dynamic (Zhu et al. 2019) and the Landsat archive held at the United States Geological Survey (USGS) Earth Resources Observation and Science (EROS) Center in 2016, when the JRC global surface water data were generated, was likely less complete than it is currently.

The use of surface reflectance (SR) data would be preferred for land cover mapping (Dong et al. 2016; Gong et al. 2019; Wang et al. 2020a; You and Dong 2020), as there are deviations between the values of these water or vegetation indices derived from TOA reflectance data and SR data (Dong et al. 2016). To date, no study has used the Landsat SR data set to generate annual maps of surface water bodies in the NCP from the 1980s to the present. The lack of information on the continuous processes of spatial–temporal dynamics of surface water bodies makes it hard to investigate the relationships between the dynamics of surface water bodies and their associated effects on regional water resources (e.g., water loss through evaporation) and the environment (e.g., greenhouse gas emissions from small ponds). Fortunately, the remote sensing cloud computing platforms (e.g., Google Earth Engine, GEE), comprising of various kinds of remote sensing (e.g., SR data of Landsat, Sentinel, and MODIS) and geospatial data sets, widely-used classifiers, and powerful computing capability (Gorelick et al. 2017; Pan et al. 2021), open opportunities for realizing retrospective and continuous monitoring of land cover changes (Dong et al. 2019; Zhou et al. 2019a). Our previous studies (Wang et al. 2020b; Zhou et al. 2019b; Zou et al. 2017; Zou et al. 2018) have documented the interannual variations of surface water bodies in the conterminous United States, China, and Mongolian Plateau by using all the available Landsat SR imagery and GEE.

This study aimed to understand the spatial–temporal changes of surface water bodies in the NCP during the past three decades and analyze the driving factors and subsequent effects on total water storage. To achieve this objective, we firstly generated the annual maps of surface water bodies at 30 m spatial resolution using all the available Landsat SR imagery and GEE, to examine the interannual variations and trends of surface water area (SWA); and then quantitatively analyzed the driving factors of the changes of SWA from both climate change and human activities; finally, we investigated the trends of water evaporation and examined the effects of SWA dynamics on total water storage. This study is expected to provide essential information for water managers and decision-makers to guide the sustainable planning and management of limited water resources in the NCP and provide a reference for the research of water resources dynamics in other similar regions over the world.

2. Materials and methods

2.1. Study area

The North China Plain (NCP) defined in this study geographically includes the municipalities of Beijing and Tianjin, and the provinces of Hebei, Henan, Shandong, and Shanxi (Fig. 1). Considering the smaller areas of Beijing and Tianjin compared to other provinces, they were merged as one region (Beijing&Tianjin, B&T) in this study. The NCP region is home to 26% of the human population in China, accounting for 25% of gross domestic production (GDP) and national grain production, but it has only 3% of the total freshwater resources (Fig. 1) (Statistics, 2019; Xu et al. 2019). Agriculture consumes more than 70% of the total water use in the region (Liu et al. 2001; Xu et al. 2005), extensive pumping for irrigation has made the region be one of the three major groundwater depletion regions in the world (Cao et al. 2013; Han et al. 2017; Huang et al. 2015; Siebert et al. 2010). In addition, the population growth and urbanization acceleration in the Beijing-Tianjin-Hebei region (Fig. 1B and C) (Yang et al. 2021; Zhao et al. 2019) aggravate the water shortage pressure in the NCP. Therefore, population growth, urbanization development, and agricultural production are likely to be limited due to the region's water scarcity (Qin et al. 2013).

2.2. Data

2.2.1. Landsat imagery

Among all the satellites, Landsat family sensors have the longest historical observations with a medium spatial resolution (Hansen and Loveland 2012; Wulder and Coops 2014), providing the most appropriate data to continuously track the dynamics of surface water bodies overtime at various spatial and temporal scales. All the available Landsat 5/7/8 Collection 1 Tier 1 SR images in the study area since 1984 were used in this study. These images were originally derived from the USGS and have been conducted geometric and atmospheric correction, as well as cross-calibration among different sensors (Dwyer et al. 2018; Wulder et al. 2016). All these images have been released in the database of GEE. In this study, the pixels of clouds, cloud shadows, and snows in each image were removed by using the quality assurance (QA) band from a cloud masking method called CFmask, which works well and is suitable for preparing Landsat data for land cover change monitoring (Zhu and Woodcock 2014). In addition, the solar azimuth and zenith angles of each image derived from image properties were used along with the digital elevation model (DEM) from Shuttle Radar Topography Mission (SRTM) to simulate and remove terrain shadows. Due to the scan line corrector (SLC)-off gaps in each Landsat 7 ETM + image after 2003, we only considered and used those good-quality observations outside the SLC-off gaps. After filtering, all these remaining pixels were considered good-quality Landsat observations, which could be used for water body detection. After a systematic and quantitative investigation towards the Landsat data availability, we found that the good-quality observations were sufficient to support retrospective and annual monitoring of surface water bodies in the NCP since 1987 (Fig. 2). Therefore, we used all the available Landsat 5/7/8 Collection 1 Tier 1 SR images covering the entire NCP during 1987–2020 (~48,000 images, ~38 terabytes of data) to continuously monitor the dynamics of SWA.
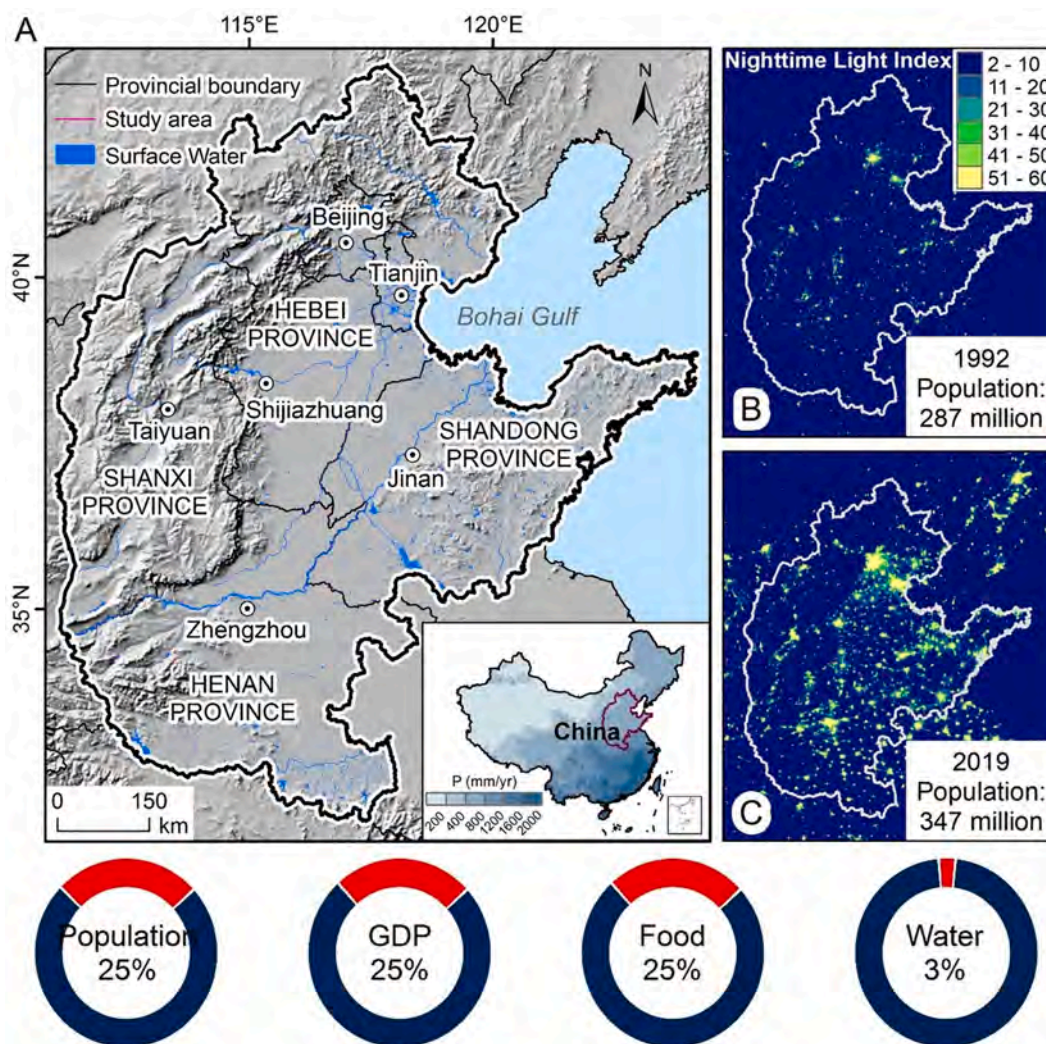
Fig. 1. Overview of the North China Plain (NCP). (A) Geographical location, climate condition, and spatial distributions of surface water bodies in the NCP. (B-C) Nighttime light index and population in the NCP in 1992 and 2019, respectively. The circular graphs showed the percentages of the total human population, GDP, food production, and freshwater resources in the NCP relative to the entire country in 2019.

2.2.2. Climate data

In this study, two kinds of long-term climate data sets were used to investigate the trends of annual precipitation (AP) in the study area during 1987–2019: the monthly 0.5° and 0.25° gridded data from the (1) Climatic Research Unit Timeseries (CRU TS) version 4.01 and (2) the fifth generation European Centre for Medium-Range Weather Forecasts (ECMWF) atmospheric reanalysis (ERA5) for the global climate, respectively. The CRU TS precipitation data set is derived from the spatial interpolation based on the daily or sub-daily observational data collected by National Meteorological Services and other agents (Shi et al. 2017), agreeing well with rain gauge measurements (Zhao et al., 2020). The ERA5, a "state-of-the-art" reanalysis precipitation data product with wide coverage and fine spatial and temporal resolutions (Xin et al. 2021), is advocated for understanding extreme precipitation and disaster events (Kumar et al. 2021). As the ERA5 climate data for July—December in 2020 has not been released, we analyzed the variations and trends of AP from 1987 to 2019. We also used the projected climate change data set in the 21st century, which were derived from Coupled Model Intercomparison Project Phase 5 (CMIP5) climate model under two Representative Concentration Pathway (RCP) scenarios: the medium greenhouse gas emission scenario RCP 4.5 and high emission scenario RCP 8.5 (https://esgf-node.llnl.gov/search/cmip5/). The spatial and temporal resolutions of the CMIP5 projected climate change

data set are 0.25° and daily. We used the CMIP5 data set to calculate AP and annual mean temperature (AMT) over the NCP in 2020–2100. The annual water evaporation was derived from the water evaporation layer in the second version of Penman-Monteith-Leuning (PML_V2) evapotranspiration (ET) data set (2000–2020), which has spatial and temporal resolutions of 500 m and eight days (Zhang et al. 2019b).

2.2.3. Reservoirs and lakes data

The data of geographical distributions of reservoirs/lakes were collected from the Global Reservoir and Dam database (GRanD), which was released by the Global Water System Project (GWSP) and the Columbia University Center for International Earth Science Information Network (CIESIN) in 2011. The reservoirs/lakes were delineated from high spatial resolution satellite imagery and are available as polygon shapefiles. The main focus of the database was to include all these reservoirs/lakes with a storage capacity of more than 0.1 km³, but many smaller reservoirs/lakes were added when remote sensing data were available (Lehner et al. 2011a, Lehner et al., 2011b). The GRand database represents the geographical distributions of global reservoirs/lakes in early 2011.

2.2.4. Statistical data

We obtained annual areas of aquaculture ponds and reservoirs/lakes
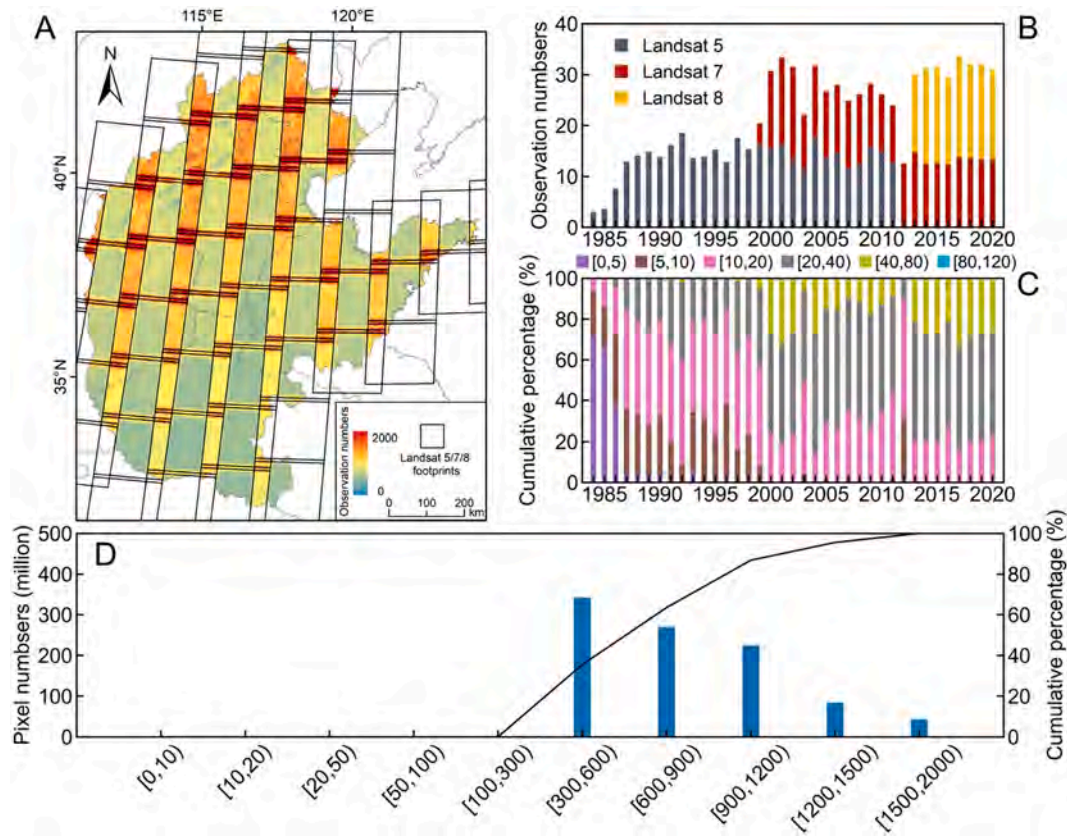
Fig. 2. Statistics of Landsat observations across the North China Plain (NCP). (A) Spatial distributions of the good-quality Landsat observations in the NCP during 1984–2020. (B) The yearly average number of the good-quality Landsat observations in the NCP during 1984–2020. (C) Cumulative percentage of Landsat pixels with the good-quality observation numbers of [0,5), [5,10), [10,20), [20,40), [40,80), [80,120), respectively, in the NCP during 1984–2020. (D) Number of Landsat pixels with the good-quality observations of [0,10), [10,20), [20,50), [50,100), [100,300), [300,600), [600,900), [900,1200), [1200,1500), [1500,2000), respectively, during 1987–2020.

in the NCP during 1987–2019 from the China Statistical Yearbook (http://www.stats.gov.cn/tjsj/ndsj/) and the statistical yearbooks of each municipality or province (https://www.yearbookchina.com/). The data for the year 2020 were not included as these statistical yearbooks of 2021 have not been released until now.

2.3. Methods

2.3.1. Satellite observations of SWA dynamics

Surface water bodies can be detected by using the relationships between water and vegetation indices, and our previous studies have performed surface water body change analyses based on time series Landsat images and the threshold-based water body mapping algorithms (Wang et al. 2020b; Zhou et al. 2019b; Zou et al. 2017; Zou et al. 2018). Similarly, the water and vegetation indices, including modified Normalized Difference Water Index (mNDWI), Enhanced Vegetation Index (EVI), and Normalized Difference Vegetation Index (NDVI), were used for surface water body mapping in this study. The complete workflow of generating annual maps of surface water bodies was shown in Fig. 3. For all the Landsat pixels with good-quality observations, these indices were calculated based on the following spectral bands and equations:

$$mNDWI = \frac{\rho_{Green} - \rho_{SWIR1}}{\rho_{Green} + \rho_{SWIR1}} \quad (1)$$

$$NDVI = \frac{\rho_{NIR} - \rho_{Red}}{\rho_{NIR} + \rho_{Red}} \quad (2)$$

$$EVI = 2.5 \times \frac{\rho_{NIR} - \rho_{Red}}{1.0 + \rho_{NIR} + 6.0\rho_{Red} + 7.5\rho_{Blue}} \quad (3)$$

where ρ_{Blue}, ρ_{Green}, ρ_{Red}, ρ_{NIR}, and ρ_{SWIR1} are the surface reflectance values of Bands blue (0.45–0.52 μm), green (0.52–0.60 μm), red (0.63–0.69 μm), near-infrared (NIR) (0.77–0.90 μm), and shortwave-infrared-1 (SWIR1) (1.55–1.75 μm), respectively, in the Landsat sensors. A criterion mNDWI > EVI or mNDWI > NDVI was used to identify the pixels which show stronger water signals than vegetation signals. EVI < 0.1 can ensure that the vegetation pixels or the mixed pixels of water and vegetation were removed. Therefore, only those pixels that meet the criteria [(mNDWI > EVI or mNDWI > NDVI) and (EVI < 0.1)] were classified as water body pixels, while other pixels were classified as non-water pixels. For each Landsat pixel in NCP, the surface water frequency in a year was calculated based on Eq. (4):

$$Frequency(y) = \frac{1}{N_y} \sum_{i=1}^{N_y} w_{y,i} \times 100\% \quad (4)$$

where Frequency is the water body frequency of a pixel, y is the specified year, N_y is the number of good-quality observations in the location in that year, $w_{y,i}$ denotes whether one observation is a water body, with "1" indicating water and "0" indicating non-water. The surface water frequencies of individual pixels in the year 2020 and the period 1987–2020 varied substantially across the entire NCP (Fig. 4A and B). After setting a certain threshold, surface water bodies were extracted from the annual maps of water body frequency, and their areas were varied according to different thresholds (Fig. 4C). In this study, SWA refers to the area of year-long surface water bodies covered by water throughout the year. A
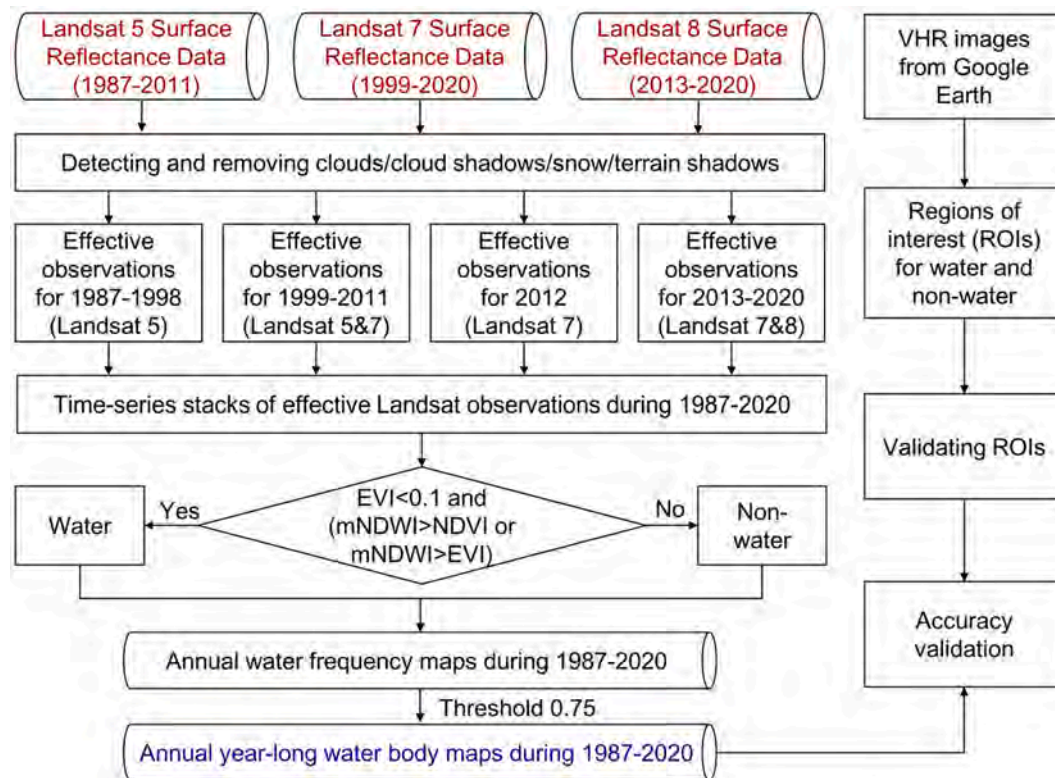
Fig. 3. Flow charts for developing annual maps of surface water bodies at spatial resolution of 30 m by using Landsat SR data.

good agreement of the interannual variations and trends of SWA between our water frequency data set with the threshold of 0.75 and JRC year-long water data set after 2000 has been observed (Fig. 4C). However, the annual SWA from our data set was higher than that from the JRC data set before 2000, when some data were missing in the JRC water data set (Wang et al. 2020b). Therefore, the water body frequency of 0.75 was set to be the threshold to extract year-long water bodies in this study, which was also consistent with our previous studies (Wang et al. 2020b; Zhou et al. 2019b; Zou et al. 2017; Zou et al. 2018).

We used the random sampling approach and very high resolution (VHR) imagery from DigitalGlobe, Centre National d'Etudes Spatiales (CNES)/Astrium at Google Earth platform to assess the accuracies of annual maps of surface water bodies. The accuracies of the year-long water body maps in 2000, 2010, and 2020 were validated. For each year, the land cover types within a total of 600 random regions of interest (ROIs) with 100 m radius circles, equal to roughly 27,000 Landsat pixels, across the entire NCP, were visually interpreted by using VHR images in Google Earth. Fig. 5 showed the spatial distributions of 169 ROIs for water and 431 ROIs for non-water which were used for accuracy assessmemt of the surface water map in 2020. In order to ensure the temporal consistency of reference data and water mapping results, we chose and interpreted the VHR images within the ROIs in the same year with the resultant maps of surface water bodies. Finally, we generated the confusion matrices for the water maps of these three years on the ENVI 5.3 platform for accuracy assessment. The results showed an overall accuracy of 97.6 % (kappa coefficient of 0.93) for the year 2000, 96.7% (0.91) for the year 2010, and 97.4% (0.93) for the year 2020, respectively (Table 1).

2.3.2. Statistical analysis of SWA dynamics

Based on the annual binary maps of surface water bodies of the NCP generated in this study, we firstly aggregated the 30 m maps into area percentage maps of SWA at both 0.5 arc degree and 1 km resolutions. We then investigated the interannual variations and trends of SWA at both pixel and regional scales. Firstly, we applied the Theil-Sen slope

estimator and the Mann-Kendall test method to annual SWA percentage maps (spatial resolutions of 0.5 arc degree and 1 km) to obtain the temporal trend of SWA and its statistical significance level in each pixel during 1987–2020. The Theil-Sen is a median-based non-parametric trend test estimator, which has no strict requirement for specific distribution of data (Yang et al. 2019). The Mann-Kendall test is a non-parametric trend test method, commonly used to detect trends in long-term time series related to the geoscience field (Forkel et al. 2015; Wang et al. 2018; Yang et al. 2019). Secondly, we investigated the interannual variations and trends of SWA in the NCP during 1987–2020 at the provincial scale using the ArcGIS 10.3 software platform and Python 2.7 programming language. Similarly, we derived the interannual variations and trends of AP and water evaporation at the pixel and regional scales.

2.3.3. Attribution analysis of SWA dynamics

Surface water bodies in the NCP mainly include rivers (e.g., Yellow River), inland reservoirs/lakes used for water conservancy projects and recreation purposes, and coastal aquaculture ponds. Therefore, the trends of SWA could be dominated by the variations of these kinds of water bodies. Here, we firstly carried out the analyses of the consistency between the spatial patterns of SWA changes and the geographical locations of the reservoirs/lakes and coastal aquaculture ponds. Secondly, we investigated the variations of anthropogenic (i.e., areas of reservoirs/lakes and aquaculture ponds) and climatic (i.e., AP) factors in the NCP. Thirdly, we applied partial correlations to quantitatively explore the effects of these factors on SWA dynamics.

2.3.4. Effects of SWA dynamics on water evaporation

Considering that surface water bodies are changing and will strongly impact the available water resources through evaporation (Zhan et al. 2019), here we quantitatively explored the effects of SWA dynamics on evaporation in the NCP through the following two steps. Firstly, we investigated and found the consistency between the spatial patterns of linear trends of water evaporation and SWA in the study area during
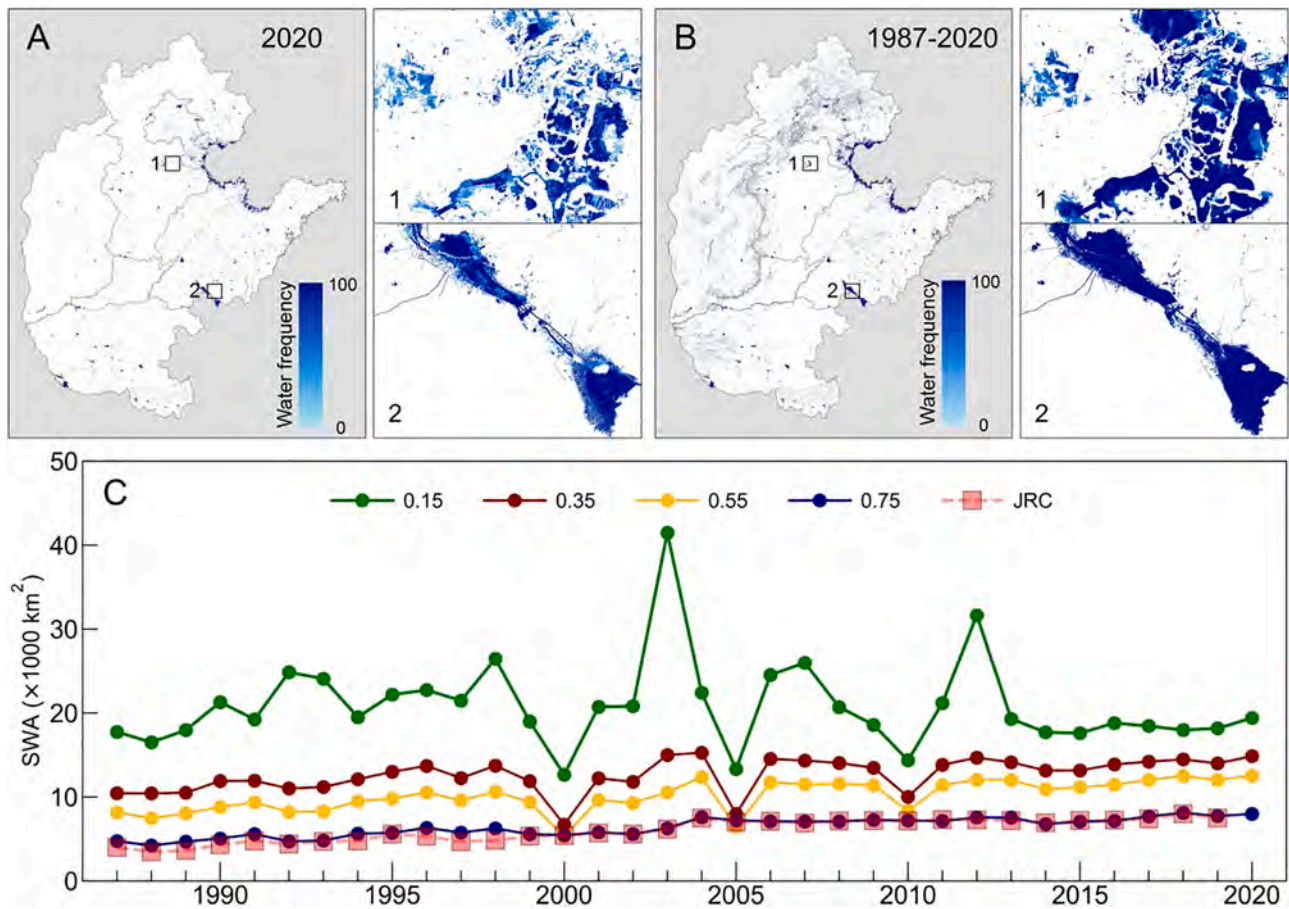
Fig. 4. Surface water body frequency maps and areas of surface water bodies by using different frequency thresholds in the NCP. (A) Surface water frequency map in the NCP in 2020, and (1, 2) are the two zoom-in views for Lake Baiyangdian in Hebei Province and Lake Nansihu in Shandong Province, respectively. (B) The 34-year surface water frequency map in the NCP during 1987–2020. (C) Annual areas of surface water bodies in the NCP during 1987–2020 with different frequency thresholds. Annual areas of permanent water bodies from the JRC data set are also shown.
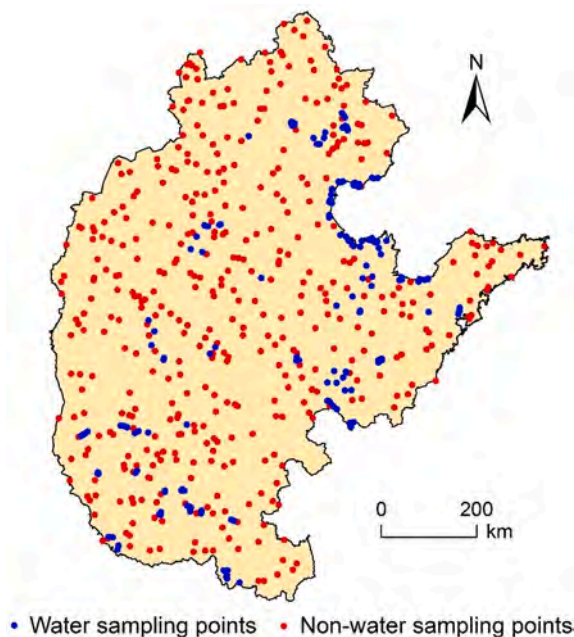
Fig. 5. Spatial distributions of 600 regions of interest (ROIs) (169 ROIs for water and 431 ROIs for non-water) in the NCP, which includes a total of ~ 27,000 pixels for accuracy assessment of the surface water map in 2020.

2000–2020. Secondly, we explored the correlation between annual total water evaporation and SWA using the linear regression model.

3. Results

3.1. Increasing SWA in the NCP from 1987 to 2020

Generally, SWA showed an increasing trend in the NCP from 1987 to 2020 (Fig. 6). Specifically, among the 336 0.5×0.5 arc degree grid cells of SWA percentage maps, 165 (49.1%) of them experienced a significant ($p < 0.05$) increase of SWA during 1987–2020 (Fig. 6A). The most remarkable expansion of SWA occurred in the eastern coastal regions and Shandong Province (Fig. 6A). Furthermore, the analyses based on higher resolution (1 km $\times$ 1 km grid cells) of SWA percentage maps showed that the large reservoirs/lakes and coastal aquaculture ponds experienced the significant expansion of SWA (Fig. 6B).

In terms of the interannual variations and trends, SWA continuously increased from 4740.0 km^2 in 1987 to 7963.7 km^2 in 2020 (increased by 68.0%) at a rate of 101.9 km^2/yr (Fig. 6C). At the provincial scale, we found that the most rapid expansion of SWA (75.0 km^2/yr) occurred in Shandong Province, followed by the provinces of Henan (16.7 km^2/yr), Hebei (8.9 km^2/yr), and Shanxi (4.8 km^2/yr). SWA of Shandong Province has more than doubled during the period, from 1469.7 km^2 in 1987 to 3586.4 km^2 in 2020 (increased by 144%). B&T is the only region that experienced the decline of SWA (-3.6 km^2/yr) during 1987–2020 (Fig. 6C). However, the trends of SWA in B&T were different in different periods. Specifically, SWA increased during 1987–1995 and then

Table 1

Confusion matrix for accuracy assessment of year-long water body maps in 2000, 2010, and 2020. The figures in confusion matrices represent the total numbers of Landsat pixels.

2000				
Classification	Ground reference		Total	User accuracy (%)
	Water	Non-water		
Water	6,324	91	6,415	98.58%
Non-water	573	20,103	20,676	97.23%
Total	6,897	20,194	27,091	Overall accuracy = 97.55%
Producer accuracy (%)	91.69%	99.55%		Kappa Coefficient = 0.93

2010				
Classification	Ground reference		Total	User accuracy (%)
	Water	Non-water		
Water	6,152	246	6,398	96.16%
Non-water	652	20,037	20,689	96.85%
Total	6,804	20,283	27,087	Overall accuracy = 96.68%
Producer accuracy (%)	90.42%	98.79%		Kappa Coefficient = 0.91

2020				
Classification	Ground reference		Total	User accuracy (%)
	Water	Non-water		
Water	7,038	207	7,245	97.14%
Non-water	513	19,377	19,890	97.42%
Total	7,551	19,584	27,135	Overall accuracy = 97.35%
Producer accuracy (%)	93.21%	98.94%		Kappa Coefficient = 0.93

decreased after 1995. It was worth noting that SWA in B&T showed an increasing trend again from 2010 to 2020 (25.9%, 21.4 km^2/yr), especially after 2014 (26.8 km^2/yr), which was the start time of the implementation of the South-to-North Water Division (SNWD) project.

3.2. SWA expansion from increasing reservoirs and aquaculture ponds

Consistent with the finding that the reservoirs/lakes and coastal aquaculture ponds have greatly expanded based on Landsat images (Fig. 6B), the statistical data about the areas of reservoirs/lakes and aquaculture ponds from the statistical yearbooks also show increasing areas of reservoirs/lakes (43.1 km^2/yr) and aquaculture ponds (64.3 km^2/yr) in the NCP during 1987–2019 (Fig. 7A and B). Human activities, including the construction and extension of inland reservoirs/lakes due to the implementation of water projects, together with aquaculture development, could contribute to the expansion of SWA. For example, the Ecological Urgent Water Replenishing (EUWR) project was implemented in Shandong Province in 2002 to divert water from the Yangtze River to sustain the Lake Nansihu (Huang 2003), while the Yellow River Division (YRD) project was implemented in Shanxi Province since 2002. The SNWD project in the provinces of Henan, Hebei, and Shandong started in 2014, which was also followed by the gradual increase of SWA. Fig. 7 showed the expansion processes of several typical inland reservoirs/lakes and aquaculture ponds, namely: Reservoir Xiaolangdi, which was used for flood and drought management and electricity production; Reservoir Dalangdian, which was used for domestic water use; Coastal aquaculture ponds in the Changzhou City of Hebei Province and Dongying City of Shandong Province. In terms of the effects of climate change on the dynamics of SWA, we found that AP (-3.3 mm/yr)

showed significantly ($p < 0.05$) negative trends during 1987–2019 (Fig. 8), which suggested that the changes in precipitation were not conducive to the increase of SWA over the past three decades.

Statistical analyses also proved that anthropogenic factors (areas of reservoirs/lakes and aquaculture ponds) played significantly positive effects on the expansion of SWA rather than precipitation. Firstly, the areas of reservoirs/lakes ($r = 0.84$, $p < 0.01$) and aquaculture ponds ($r = 0.84$, $p < 0.01$) were significantly and positively correlated with SWA expansion during 1987–2019, while AP ($r = -0.2$, $p = 0.27$) was not significantly correlated with SWA changes (Fig. 9). Secondly, partial correlations indicated that the relationship between the areas of reservoirs/lakes and SWA remains significant after controlling for the effect of AP. However, controlling for the effect of the areas of aquaculture ponds strongly decreases partial correlation between the areas of reservoirs/lakes and SWA, which suggested that most of the information on SWA variations that are contained in the areas of reservoirs/lakes can be found in the areas of aquaculture ponds. The partial correlations between the areas of aquaculture ponds and SWA were similar to those between the areas of reservoirs/lakes and SWA. These statistical analyses suggested that the expansion of SWA was mainly controlled by the increases of the areas of aquaculture ponds and reservoirs/lakes rather than the changes of AP.

3.3. Increasing water evaporation and potential effects on regional water storage

Fig. 10 showed the spatial patterns of linear trends of SWA (spatial resolution of 1 km) and water evaporation (1 km and 0.5 arc degree) in the NCP during 2000–2020. As can be seen, the regions (i.e., reservoirs/lakes, coastal aquaculture ponds) with SWA expansion experienced significant increases in water evaporation during 2000–2020 (Fig. 10A and B). The increases of evaporation were the most remarkable in the eastern parts of NCP, especially in Shandong Province (Fig. 10C), coinciding with the most rapid expansion of SWA in the province (Fig. 6). The total water evaporation significantly increased at a rate of 0.09 km^3/yr in the NCP during 2000–2020 (Fig. 10D). The linear regression between the changes of water evaporation and SWA showed that there was a significant ($p < 0.01$) and positive correlation between the increase of total water evaporation and expansion of SWA (Fig. 10E). The consistent spatial patterns of water evaporation rise and SWA expansion, together with the significant correlation between the interannual variations of water evaporation and SWA, suggested that the expansion of SWA greatly contributed to the increases of water evaporation in the NCP.

Considering that Shandong Province experienced the most rapid increases in SWA and water evaporation, we also quantitatively studied the effects of water evaporation increase on total water storage in Shandong. The results showed that annual total water evaporation significantly increased at a rate of 0.03 km^3/yr in Shandong Province during 2000–2020 (Fig. 10F), and there was a significant ($p < 0.01$) and positive correlation between the increase of water evaporation and expansion of SWA (Fig. 10G). The annual increase of water evaporation in Shandong was equivalent to a loss of total water storage by 0.25 mm/yr in the province. For the regions covered by surface water bodies in Shandong in 2000 (2085 km^2), the annual increase of water evaporation was equivalent to water storage decline by 14.4 mm; while for the surface water regions in 2020 (3586 km^2), annual water evaporation increase was equal to water storage decline by 8.4 mm. Therefore, the increasing evaporation due to SWA expansion could accelerate the loss of water storage at a rate of 8.4–14.4 mm/yr in the surface water regions in Shandong Province during 2000–2020.
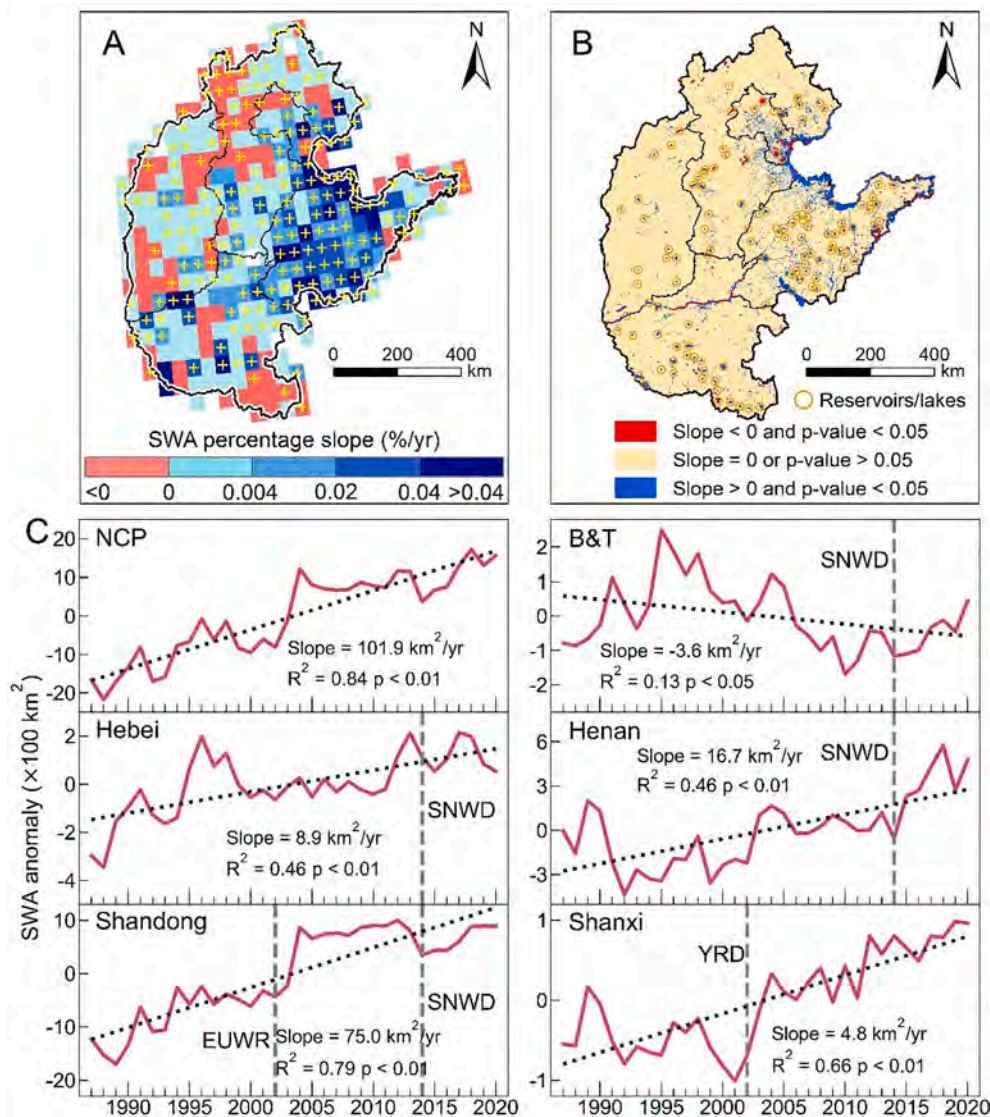
Fig. 6. Trends and interannual variations of SWA in the NCP during 1987–2020. Spatial patterns of linear trends of SWA percentage at 0.5 arc degree (A) and 1 km (B) resolutions in the NCP during 1987–2020, respectively; (c) Interannual variations of SWA in the whole NCP and different provinces during 1987–2020. The symbol "+" in each grid cell indicates a statistically significant trend with a *p*-value < 0.05. The grey dotted lines represent major water projects of the South-to-North Water Division (SNWD) project, Ecological Urgent Water Replenishing (EUWR) project, and Yellow River Division (YRD) project. (For interpretation of the references to colour in this figure legend, the reader is referred to the web version of this article.)

4. Discussion

4.1. Implications of expanded SWA in the NCP

Despite the long-term severe water shortage in the NCP, this study revealed the expanded areas of surface water bodies in the region over the past three decades. The expansion of SWA is of great significance to human well-being and ecosystem in such a water-limited region because: (1) the widely distributed reservoirs/lakes ensure water supply to industrial and agricultural production and domestic uses (Gao et al. 2017; O'Reilly et al. 2015); (2) some large lakes (e.g., Lake Baiyangdian) coupled with its surrounding runoff are internationally important wetlands, playing a vital role in protecting biodiversity and maintaining ecosystem by providing habitats for a wide range of precious species (Liu et al. 2013; Tao et al. 2015b); (3) the construction of urban artificial lakes provide recreation landscapes for residents.

However, some ecological and environmental issues brought by the expanded SWA can not be ignored. Firstly, previous studies (Jia et al. 2021; Mao et al. 2018; Ren et al. 2019) have documented that the transformation of wetlands to aquaculture ponds in coastal regions of the NCP damaged the habitats of coastal mangroves and reeds as well as numerous precious fish and endangered migratory birds (Jiang et al. 2015). Secondly, aquaculture ponds greatly contributed to greenhouse

gas emissions (Holgerson and Raymond 2016; Wik et al. 2016), and affected local water quality through the use of artificial feed and chemical additives (Pattanaik and Narendra Prasad, 2011). Thirdly, as the water in some lakes or reservoirs is extracted from underground aquifers, the exposure of groundwater to the surface could increase water evaporation, and therefore strongly impact the regional water resources (Zhan et al. 2019). In this study, we found consistent spatial patterns and a significant correlation between water evaporation increase and SWA expansion, as the shallow nature of these artificial reservoirs/lakes and aquaculture ponds could cause excess evaporation because of the frequent heating and cooling cycles due to their limited abilities to store energy (Sacks et al. 1994). This study suggests that the expansion of surface water bodies could accelerate the loss of regional water resources through evaporation. Finally, the increase of reservoir numbers could cause the loss of river connectivity and threaten the ecosystem process these rivers support (Grill et al. 2019).

4.2. Effects of future climate on surface water resources

Future climate change could significantly affect the long-term variations of surface water bodies. Therefore, understanding the trends of climate conditions in the future is of great significance to sustainable management and the use of water resources. Using the CMIP5 projected
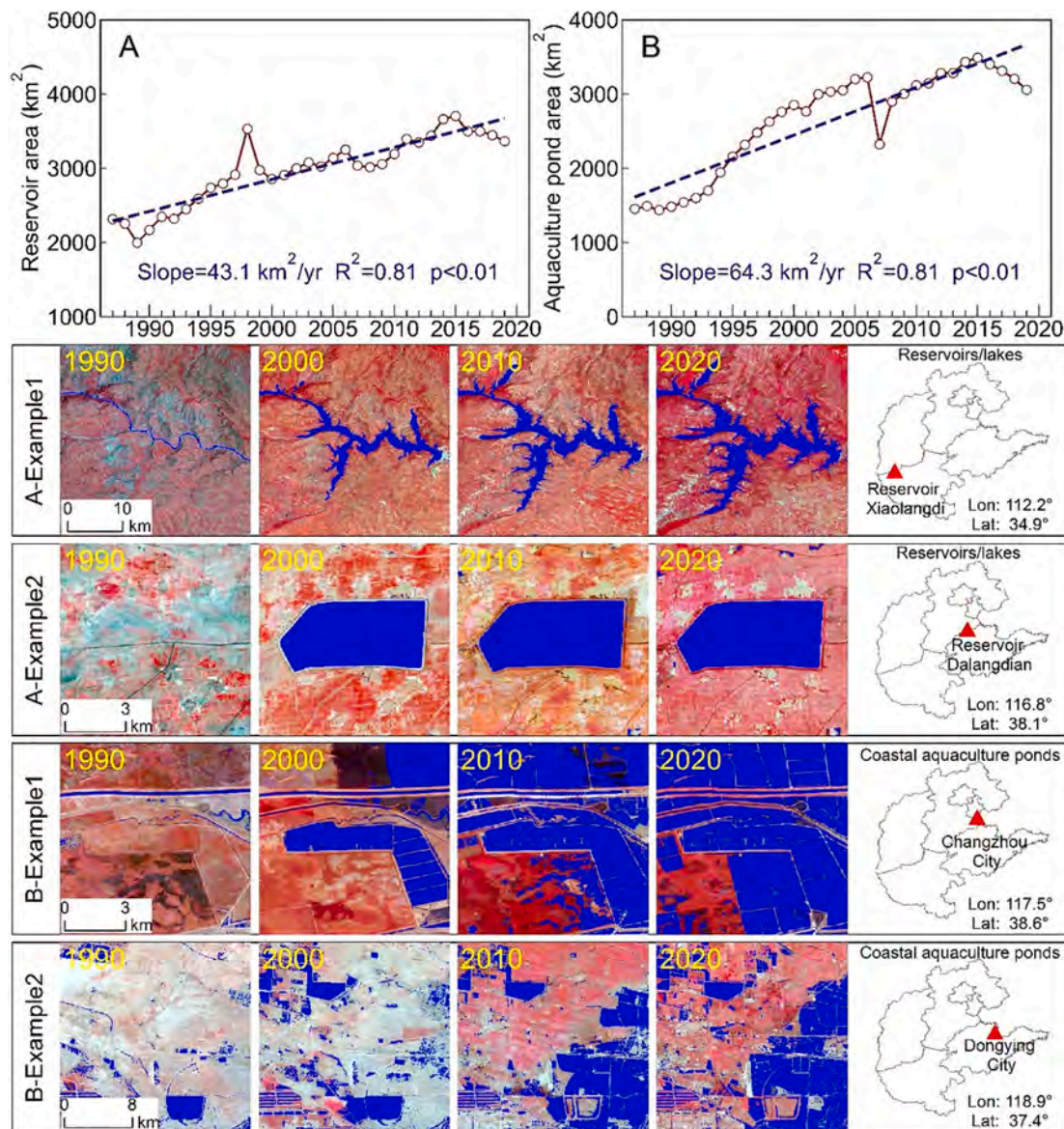
Fig. 7. Interannual variations and trends of the areas of reservoirs/lakes (A) and aquaculture ponds (B) in the NCP during 1987–2019 from the statistical data. The bottom Landsat images showed the expansion processes of several artificial reservoirs/lakes and aquaculture ponds, namely: Reservoir Xiaolangdi (A-Example1) in the Luoyang City of Henan Province, Reservoir Dalangdian (A-Example2) in the Changzhou City of Hebei Province, and typical coastal aquaculture ponds in the Changzhou City of Hebei Province (B-Example1) and Dongying City of Shandong Province (B-Example2).

data under both medium (RCP 4.5) and high (RCP 8.5) greenhouse gas emission scenarios, the trends of temperature and precipitation in the NCP from 2020 to 2100 were investigated. The results showed that both the precipitation and temperature would increase in the region in the future under these scenarios. The annual mean of daily-minimum temperature will significantly ($p < 0.01$) increase at a rate of 0.02 °C/yr and 0.03 °C/yr under the scenarios of RCP 4.5 and RCP 8.5, respectively (Fig. 11); while the annual mean of daily-maximum temperature will significantly increase at a rate of 0.06 °C/yr for both the two scenarios. The RCP 4.5 projected the lowest increase of AP (0.52 mm/yr, $p < 0.01$), while the RCP 8.5 projected the highest increase (1.19 mm/yr, $p < 0.01$).

Raising temperature is likely to affect ET and atmospheric water storage, and thereby the precipitation (Salem et al. 2018). Continuous temperature rise in the future could further stress the pressure of water shortage in the NCP, and bring considerable threats to natural ecosystem and restrict regional sustainable development. On the one hand, the increasing temperature could cause more consumption of surface water resources by agricultural irrigation (Zhang et al. 2019c); On the other

hand, more substantial water evaporation induced by higher temperatures would lead to the decline of surface water resources and even the drying out of runoff and wetlands, and consequently affect the biodiversity in riparian or wetland ecosystems. Therefore, the water resource crisis of the NCP would continue in the future, and effective water-saving measures are urgent.

4.3. Comparison with previous studies

For such a water-limited region of the NCP, previous studies mainly focused on the dynamics of groundwater resources and total water storage. Using the data of Gravity Recovery and Climate Experiment (GRACE), previous studies (Aeschbach-Hertig and Gleeson 2012; Pan et al. 2017; Qin et al. 2013) have revealed that the NCP was one of the three most serious depletion hotspots of water storage in the world, and identified the intense agricultural irrigation as the main driving factor of the depleting water storage in the NCP in the past decades. For example, Huang et al. (2015) detected the variations of groundwater storage in
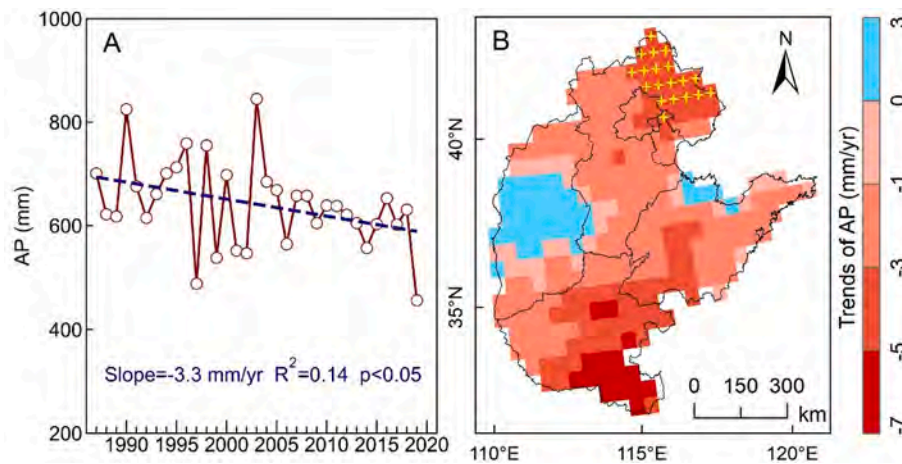
Fig. 8. Interannual variations and trends of annual precipitation (AP) from CRU and ERA5 climate data in the NCP during 1987–2019. (A) Interannual variations and trends of AP at the provincial scale. (B) Spatial patterns of linear trends of AP at pixel scale of 0.5 arc degree. The symbol "+" in each grid cell indicates a statistically significant trend with a *p*-value < 0.05.
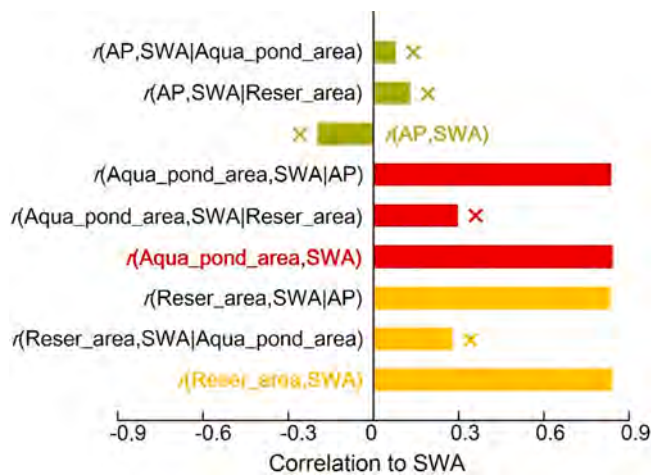
Fig. 9. Correlations and partial correlations between anthropogenic or climatic factors and SWA changes. Shown in yellow, from bottom to top, is first the correlation between reservoir/lake area (Reser_area) and SWA, followed by partial correlations r between Reser_area and SWA after controlling for the effect of aquaculture pond area (Aqua_pond_area) and AP. Shown in red, from bottom to top, is first the correlation between Aqua_pond_area and SWA, followed by partial correlations r between Aqua_pond_area and SWA after controlling for the effect of Reser_area and AP. Shown in light green, from bottom to top, is first the correlation between AP and SWA, followed by partial correlations r between AP and SWA after controlling for the effect of Reser_area and Aqua_pond_area. Each cross symbol indicates that the trend was not statistically significant ($p \geq 0.05$). (For interpretation of the references to colour in this figure legend, the reader is referred to the web version of this article.)

the NCP during 2003–2013 and found the depleted groundwater storage (>16 mm/yr) owing to groundwater overexploitation; Xu et al. (2019) revealed the decline of total water storage (>7 mm/yr) in the region from 2003 to 2016 due to agricultural irrigation.

Surface water is also an important component of total water storage. Though previous studies (Pekel et al. 2016; Song et al. 2018; Tao et al. 2015b; Wang et al. 2020b; Zhang et al. 2019a; Zhang et al. 2017; Zhou et al. 2019b; Zou et al. 2018) have investigated the dynamics of surface water bodies, they only focused on the variations and trends of surface water bodies as well as their driving factors; the studies about the effects of the dynamics of surface water bodies on total water storage are still very limited. For example, Zhang et al. (2019a) investigated the changes of lakes in China over eight periods (every five or ten years for a period)

during 1960s—2015 by using Landsat TOA images and topographic maps. However, they only focused on the dynamics of lakes with sizes over 1 km². In addition, the epoch-based analyses of lake dynamics could miss important information (e.g., turning points) about the inter-annual variations of surface water bodies due to their strong variability. Similar studies included the analyses of lake dynamics in the Tibetan Plateau (Zhang et al. 2017) and Mongolian Plateau (Tao et al. 2015b) during several sparse epochs. In contrast, our current study could depict the complete processes of SWA dynamics in the NCP from 1987 to the present. Though our previous study (Wang et al. 2020b) investigated the interannual variations and spatial patterns of trends of SWA and total water storage in China during 1989–2016, and revealed the spatial–temporal divergency and consistency between SWA and total water storage in the whole country. However, that study focused on analyzing water resources dynamics at the national scale, lacking the quantitative analyses of the effects of SWA dynamics on total water storage in the NCP.

In this study, we firstly investigated the continuous change processes of SWA and their driving factors in the NCP from 1987 to the present using all the available Landsat SR data and GEE. We then quantitatively analyzed the effects of SWA dynamics on total water storage by investigating the relationships between the changes of SWA and water evaporation. We found that the expanded SWA due to the increasing artificial reservoirs and aquaculture ponds could accelerate the loss of water in the NCP through increased evaporation (0.09 km³/yr). The data and methods used in this study to continuously monitor the dynamics of surface water bodies and explore the effects of SWA changes on total water storage are also applicable to similar researches in other regions across the globe.

4.4. Uncertainties and limitations in this study

Though our current study, together with previous researches (Pekel et al. 2016; Song et al. 2018; Tao et al. 2015a; Wang et al. 2020b; Zhang et al. 2019a; Zhang et al. 2017; Zhou et al. 2019b; Zou et al. 2018), have contributed to the research progresses of water resources changes, we have to note that there are still uncertainties and limitations remained in the methods and analyses in this study. The uncertainties of the methods, remote sensing data, and those ancillary data (ET and precipitation) used in this study were analyzed. Firstly, surface water body mapping using 30 m spatial resolution Landsat imagery could miss some water bodies with sizes smaller than 30 m × 30 m. Secondly, some bad-quality observations (e.g., clouds, terrain shadows, snows) may remain after quality filtering, which might have led to some low-frequency
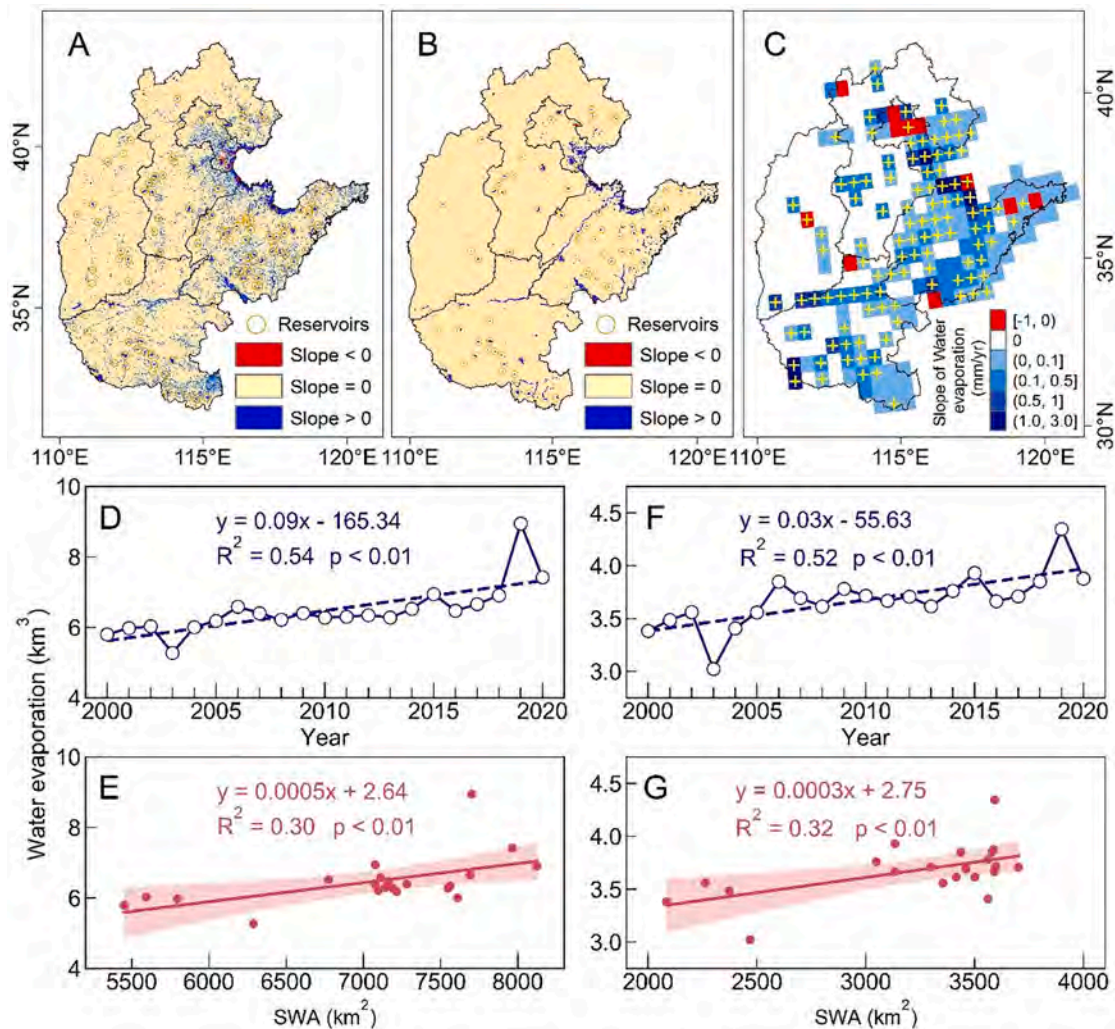
Fig. 10. Trends of SWA and water evaporation in the NCP during 2000–2020. Spatial patterns of linear trends of SWA at the spatial resolution of 1 km (A) in the NCP during 2000–2020; Spatial patterns of linear trends of water evaporation at the spatial resolutions of 1 km (B) and 0.5 arc degree (C) in the NCP during 2000–2020, respectively; The symbol "+" in each grid cell indicates a statistically significant trend with a p-value < 0.05; (D) Interannual variations of total water evaporation in the NCP during 2000–2020; (E) Linear trends between SWA and total water evaporation in the NCP during 2000–2020; (F) Interannual variations of total water evaporation in Shandong Province during 2000–2020; (G) Linear trends between SWA and total water evaporation in Shandong Province during 2000–2020.

inundation noises in the water body maps (Wang et al. 2020b). Therefore, the spatial–temporal dynamics of year-long surface water bodies in this study can provide much more reliable information than that of seasonal water bodies. In addition, it should be noted that some other satellite data (e.g., Sentinel-2) with higher spatial resolutions have been released in GEE. The virtual constellation of Landsat with these sensors could provide observations with both high spatial and temporal resolutions for continuous monitoring of water body dynamics (Wulder et al. 2015; Zhou et al. 2019b). Finally, we used the Theil-Sen slope estimator and the Mann-Kendall test method to investigate the spatial patterns of linear trends of SWA in the NCP during 1987–2020. However, it is notable that some abrupt changes are not likely to be reflected in SWA trends, especially in the early or late of the time series.

The use of those climate data products to analyze the driving factors of SWA dynamics and their effects on total water storage could also bring some uncertainties to the studies. Though PML_V2 ET data were modeled by using Penman-Monteith (PM) equation and taking MODIS data (albedo, emissivity, and leaf area index) and GLDAS meteorological forcing data as input data (Zhang et al. 2019b), this data set has been recognized as one of the most advanced and popular sources for actual values of ET and evaporation, and compared favorably with several eddy covariance flux towers (Fuentes et al. 2020). For example, He et al.

(2020) verified and compared the three high-resolution ET products (PML_V2, SSEBop_V4, and MOD16A2) in North China, and found that PML_V2 showed the highest consistency with the fluctuation trend observed at the site. The combined use of the two data sets with different spatial resolutions could also bring some uncertainties to the trends of precipitation, as there are inevitable deviations in generating these two kinds of precipitation data sets of CRU TS and ERA5. However, they are commonly used data products and have been widely applied in researches related to climate change (Ukkola et al. 2020; Zhang et al. 2017; Zhang et al. 2020) and hydrology and water resources (Li et al. 2018; Sharma et al. 2019; Xu et al. 2019; Zhao et al., 2020).

In addition, we need to recognize that the water indices- and threshold-based water mapping algorithm used in this study can only detect surface water bodies. Given that wetlands not only refer to the regions covered by surface water bodies but also the surrounding vegetated regions and the mixes of water and vegetation (Li et al. 2021; Liu et al. 2020; Mao et al. 2020). The extensive applications of the algorithm in monitoring the dynamics of wetlands should consider the seasonality of the composites of water and vegetation; thus, the algorithms should be modified accordingly.
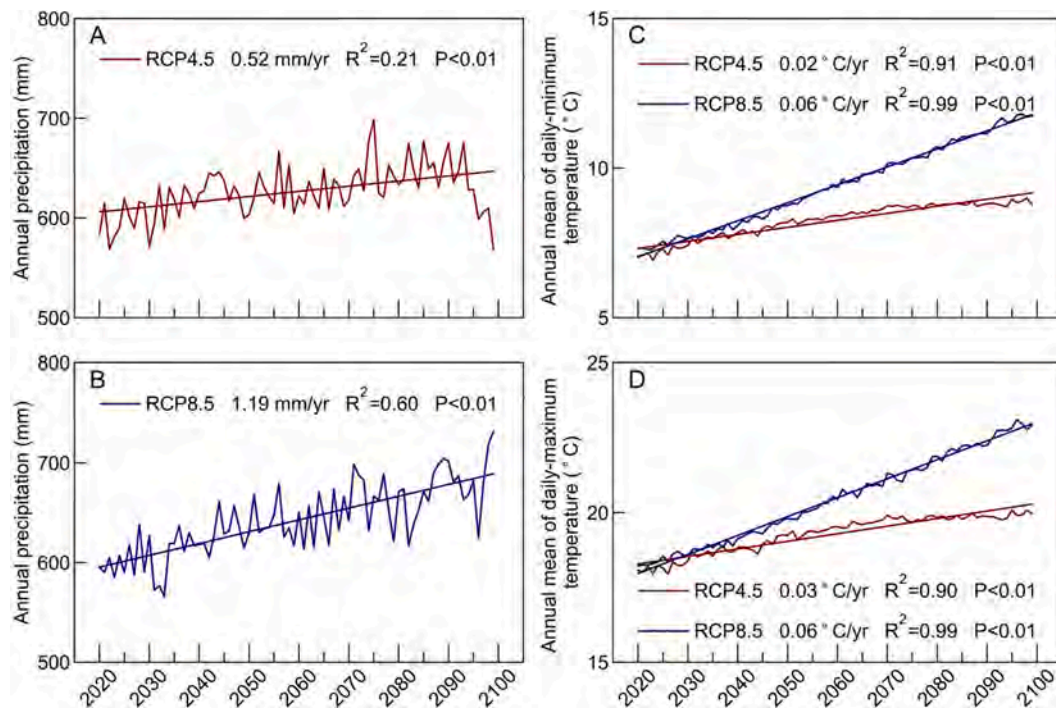
Fig. 11. Future climate projection in the NCP. Trends of annual precipitation in 2020–2099 based on the CMIP5 projected data under RCP 4.5 (A) and RCP 8.5 (B) scenarios. Trends of an annual mean of daily-minimum (C) and daily-maximum (D) temperature in the NCP in 2020–2099 under RCP 4.5 and RCP 8.5 scenarios.

5. Conclusion

The NCP is one of the most important agricultural production regions and densely populated areas in China. Using all the available Landsat imagery, water indices- and threshold-based water mapping algorithm, and cloud computing platform GEE, this study investigated the inter-annual variations and trends of SWA in the NCP from 1987 to 2020. We showed that SWA in the NCP significantly increased from 4740.0 km^2 in 1987 to 7963.7 km^2 in 2020 (increased by 68.0%) at a rate of 101.9 km^2/yr. Shandong Province experienced the most remarkable increase of SWA (75.0 km^2/yr), followed by the provinces of Henan (16.7 km^2/yr), Hebei (8.9 km^2/yr), and Shanxi (4.8 km^2/yr). B&T is the only region that experienced a decrease in SWA (-3.6 km^2/yr). We found that the increasing reservoirs/lakes owing to the implementation of water projects, together with aquaculture development, were the main drivers for the expansion of SWA in the NCP. In addition, the water evaporation significantly increased at a rate of 0.09 km^3/yr in the NCP during 2000–2020. Also, Shandong Province experienced the most rapid increase in water evaporation (0.03 km^3/yr) as the shallow nature of these artificial reservoirs/lakes and aquaculture ponds could cause excess evaporation because of the frequent heating and cooling cycles due to their limited abilities to store energy, which could accelerate the loss of water resources at a rate of 8.4–14.4 mm/yr in the regions covered by surface water bodies. The CMIP5 future climate projections revealed a significant temperature increase (0.02–0.06 °C/yr) but a small change in precipitation under both RCP 4.5 and RCP 8.5 scenarios, which indicated that the future climate change would add a new threat to water security in the NCP.

CRediT authorship contribution statement

Yan Zhou: Conceptualization, Methodology, Formal analysis, Writing – original draft. **Jinwei Dong:** Supervision, Conceptualization, Writing – review & editing. **Yaoping Cui:** Data curation, Writing – review & editing. **Sha Zhou:** Data curation, Writing – review & editing. **Zhichao Li:** Writing – review & editing. **Xinxin Wang:** Writing – review & editing. **Xiangzheng Deng:** Writing – review & editing. **Zhenhua**

Zou: Writing – review & editing. **Xiangming Xiao:** Supervision, Writing – review & editing.

Declaration of Competing Interest

The authors declare that they have no known competing financial interests or personal relationships that could have appeared to influence the work reported in this paper.

Acknowledgments

References

Aeschbach-Hertig, W., Gleeson, T., 2012. Regional strategies for the accelerating global problem of groundwater depletion. Nat. Geosci. 5 (12), 853–861.
Cao, G., Zheng, C., Scanlon, B.R., Liu, J., Li, W., 2013. Use of flow modeling to assess sustainability of groundwater resources in the North China Plain. Water Resour. Res. 49 (1), 159–175.
Dong, J., Xiao, X., Menarguez, M.A., Zhang, G., Qin, Y., Thau, D., Biradar, C., Moore, B., 2016. Mapping paddy rice planting area in northeastern Asia with Landsat 8 images, phenology-based algorithm and Google Earth Engine. Remote Sens. Environ. 185, 142–154.
Dong, J., Metternicht, G., Hostert, P., Fensholt, R., Chowdhury, R.R., 2019. Remote sensing and geospatial technologies in support of a normative land system science: status and prospects. Curr. Opin. Environ. Sustainability 38, 44–52.
Dwyer, J.L., Roy, D.P., Sauer, B., Jenkerson, C.B., Zhang, H.K.K., Lymburner, L., 2018. Analysis ready data: enabling analysis of the landsat archive. Remote Sens. 10 (9), 1363.
Forkel, M., Migliavacca, M., Thonicke, K., Reichstein, M., Schaphoff, S., Weber, U., Carvalhais, N., 2015. Codominant water control on global interannual variability and trends in land surface phenology and greenness. Glob. Change Biol. 21 (9), 3414–3435.
Fuentes, I., van Ogtrop, F., Vervoort, R.W., 2020. Long-term surface water trends and relationship with open water evaporation losses in the Namoi catchment, Australia. J. Hydrol. 584, 124714.
Gao, H., Ryan, M.C., Li, C., Sun, B., 2017. Understanding the role of groundwater in a remote transboundary Lake (Hulun Lake, China). Water 9 (6), 363.

Gong, P., Li, X., Zhang, W., 2019. 40-Year (1978–2017) human settlement changes in China reflected by impervious surfaces from satellite remote sensing. Sci. Bull. 64 (11), 756–763.

Gorelick, N., Hancher, M., Dixon, M., Ilyushchenko, S., Thau, D., Moore, R., 2017. Google Earth Engine: planetary-scale geospatial analysis for everyone. Remote Sens. Environ. 202, 18–27.

Grill, G., Lehner, B., Thieme, M., Geenen, B., Tickner, D., Antonelli, F., Babu, S., Borrelli, P., Cheng, L., Crochetiere, H., Ehalt Macedo, H., Filgueiras, R., Goichot, M., Higgins, J., Hogan, Z., Lip, B., McClain, M.E., Meng, J., Mulligan, M., Nilsson, C., Olden, J.D., Opperman, J.J., Petry, P., Reidy Liermann, C., Sáenz, L., Salinas-Rodríguez, S., Schelle, P., Schmitt, R.J.P., Snider, J., Tan, F., Tockner, K., Valdujo, P. H., van Soesbergen, A., Zarfl, C., 2019. Mapping the world's free-flowing rivers. Nature 569 (7755), 215–221.

Guo, Y., Shen, Y., 2015. Quantifying water and energy budgets and the impacts of climatic and human factors in the Haihe River Basin, China: 1. Model and validation. J. Hydrol. 528, 206–216.

Hall, J.W., Grey, D., Garrick, D., Fung, F., Brown, C., Dadson, S.J., Sadoff, C.W., 2014. Coping with the curse of freshwater variability. Science 346 (6208), 429–430.

Han, S.J., Tian, F.Q., Liu, Y., Duan, X.H., 2017. Socio-hydrological perspectives of the co-evolution of humans and groundwater in Cangzhou, North China Plain. Hydrol. Earth Syst. Sci. 21 (7), 3619–3633.

Hansen, M.C., Loveland, T.R., 2012. A review of large area monitoring of land cover change using Landsat data. Remote Sens. Environ. 122, 66–74.

He, S.Y., Tian, J., Zhang, Y.Q., 2020. Verification and comparison of three high-resolution surface evapotranspiration products in North China. Resour. Sci. 42 (10), 2035–2046.

Holgerson, M.A., Raymond, P.A., 2016. Large contribution to inland water CO2 and CH4 emissions from very small ponds. Nat. Geosci. 9 (3), 222–226.

Huang, H., 2003. Analysis of Ecological Urgent Water Replenishing From the Yangtze River to Nansihu Lake. South-to-North Water Trans. Water Sci. Technol. 1, 22–25.

Huang, C., Chen, Y., Zhang, S., Wu, J., 2018. Detecting, extracting, and monitoring surface water from space using optical sensors: a review. Rev. Geophys. 56 (2), 333–360.

Huang, Z., Pan, Y., Gong, H., Yeh, P.-F., Li, X., Zhou, D., Zhao, W., 2015. Subregional-scale groundwater depletion detected by GRACE for both shallow and deep aquifers in North China Plain. Geophys. Res. Lett. 42 (6), 1791–1799.

Ji, L.Y., Gong, P., Wang, J., Shi, J.C., Zhu, Z.L., 2018. Construction of the 500-m Resolution Daily Global Surface Water Change Database (2001–2016). Water Resour. Res. 54 (12), 10270–10292.

Jia, M., Wang, Z., Mao, D., Ren, C., Wang, C., Wang, Y., 2021. Rapid, robust, and automated mapping of tidal flats in China using time series Sentinel-2 images and Google Earth Engine. Remote Sens. Environ. 255, 112285.

Jiang, T.-T., Pan, J.-F., Pu, X.-M., Wang, B.o., Pan, J.-J., 2015. Current status of coastal wetlands in China: degradation, restoration, and future management. Estuar. Coast. Shelf Sci. 164, 265–275.

Kumar, M., Hodnebrog, Ø., Sophie Daloz, A., Sen, S., Badiger, S., Krishnaswamy, J., 2021. Measuring precipitation in Eastern Himalaya: ground validation of eleven satellite, model and gauge interpolated gridded products. J. Hydrol. 599, 126252.

Lehner, B., Reidy Liermann, C., Revenga, C., Vorosmarty, C., Fekete, B., Crouzet, P., et al., 2011. Global Reservoir and Dam Database, Version 1 (GRanDv1): Reservoirs, Revision 01. In. Palisades, NY: NASA Socioeconomic Data and Applications Center (SEDAC).

Lehner, B., Liermann, C.R., Revenga, C., Vörösmarty, C., Fekete, B., Crouzet, P., Döll, P., Endejan, M., Frenken, K., Magome, J., Nilsson, C., Robertson, J.C., Rödel, R., Sindorf, N., Wisser, D., 2011b. High-resolution mapping of the world's reservoirs and dams for sustainable river-flow management. Front. Ecol. Environ. 9 (9), 494–502.

Li, Y., Piao, S., Li, L.Z.X., Chen, A., Wang, X., Ciais, P., Huang, L., Lian, X.u., Peng, S., Zeng, Z., Wang, K., Zhou, L., 2018. Divergent hydrological response to large-scale afforestation and vegetation greening in China. Sci. Adv. 4 (5) eaar4182.

Li, Y., Mao, D., Wang, Z., Wang, X.i., Tan, X., Jia, M., Ren, C., 2021. Identifying variable changes in wetlands and their anthropogenic threats bordering the Yellow Sea for water bird conservation. Global Ecol. Conserv. 27, e01613.

Liu, Q., Liu, J., Liu, H., Liang, L., Cai, Y., Wang, X., Li, C., 2020. Vegetation dynamics under water-level fluctuations: implications for wetland restoration. J. Hydrol. 581, 124418.

Liu, H., Yin, Y.i., Piao, S., Zhao, F., Engels, M., Ciais, P., 2013. Disappearing lakes in semiarid Northern China: drivers and environmental impact. Environ. Sci. Technol. 47 (21), 12107–12114.

Liu, C.M., Yu, J.J., Kendy, E., 2001. Groundwater exploitation and its impact on the environment in the North China Plain. Water Int. 26 (2), 265–272.

Mao, D., Wang, Z., Wu, J., Wu, B., Zeng, Y., Song, K., Yi, K., Luo, L., 2018. China's wetlands loss to urban expansion. Land Degrad. Dev. 29 (5), 2644–2657.

Mao, D., Wang, Z., Du, B., Li, L., Tian, Y., Jia, M., Zeng, Y., Song, K., Jiang, M., Wang, Y., 2020. National wetland mapping in China: a new product resulting from object-based and hierarchical classification of Landsat 8 OLI images. ISPRS J. Photogramm. Remote Sens. 164, 11–25.

O'Reilly, C.M., Sharma, S., Gray, D.K., Hampton, S.E., Read, J.S., Rowley, R.J., et al., 2015. Rapid and highly variable warming of lake surface waters around the globe. Geophys. Res. Lett. 42 (24), 10773–10781.

Pan, L.i., Xia, H., Yang, J., Niu, W., Wang, R., Song, H., Guo, Y., Qin, Y., 2021. Mapping cropping intensity in Huaihe basin using phenology algorithm, all Sentinel-2 and Landsat images in Google Earth Engine. Int. J. Appl. Earth Obs. Geoinf. 102, 102376.

Pan, Y., Zhang, C., Gong, H., Yeh, P.-F., Shen, Y., Guo, Y., Huang, Z., Li, X., 2017. Detection of human-induced evapotranspiration using GRACE satellite observations in the Haihe River basin of China. Geophys. Res. Lett. 44 (1), 190–199.

Pattanaik, C., Narendra Prasad, S., 2011. Assessment of aquaculture impact on mangroves of Mahanadi delta (Orissa), East coast of India using remote sensing and GIS. Ocean Coast. Manag. 54 (11), 789–795.

Pekel, J.-F., Cottam, A., Gorelick, N., Belward, A.S., 2016. High-resolution mapping of global surface water and its long-term changes. Nature 540 (7633), 418–422.

Qin, H., Cao, G., Kristensen, M., Refsgaard, J.C., Rasmussen, M.O., He, X., Liu, J., Shu, Y., Zheng, C., 2013. Integrated hydrological modeling of the North China Plain and implications for sustainable water management. Hydrol. Earth Syst. Sci. 17 (10), 3759–3778.

Ren, C., Wang, Z., Zhang, Y., Zhang, B., Chen, L., Xi, Y., Xiao, X., Doughty, R.B., Liu, M., Jia, M., Mao, D., Song, K., 2019. Rapid expansion of coastal aquaculture ponds in China from Landsat observations during 1984–2016. Int. J. Appl. Earth Obs. Geoinf. 82, 101902.

Sacks, L.A., Lee, T.M., Radell, M.J., 1994. Comparison of energy-budget evaporation losses from two morphometrically different Florida seepage lakes. J. Hydrol. 156 (1-4), 311–334.

Salem, G.S.A., Kazama, S.o., Shahid, S., Dey, N.C., 2018. Impacts of climate change on groundwater level and irrigation cost in a groundwater dependent irrigated region. Agric. Water Manag. 208, 33–42.

Sharma, S., Blagrave, K., Magnuson, J.J., O'Reilly, C.M., Oliver, S., Batt, R.D., Magee, M. R., Straile, D., Weyhenmeyer, G.A., Winslow, L., Woolway, R.I., 2019. Widespread loss of lake ice around the Northern Hemisphere in a warming world. Nat. Clim. Change 9 (3), 227–231.

Shi, H., Li, T., Wei, J., 2017. Evaluation of the gridded CRU TS precipitation dataset with the point raingauge records over the Three-River Headwaters Region. J. Hydrol. 548, 322–332.

Siebert, S., Burke, J., Faures, J.M., Frenken, K., Hoogeveen, J., Döll, P., Portmann, F.T., 2010. Groundwater use for irrigation - a global inventory. Hydrol. Earth Syst. Sci. 14 (10), 1863–1880.

Song, C., Huang, B.o., Ke, L., 2013. Modeling and analysis of lake water storage changes on the Tibetan Plateau using multi-mission satellite data. Remote Sens. Environ. 135, 25–35.

Song, C., Ke, L., Pan, H., Zhan, S., Liu, K., Ma, R., 2018. Long-term surface water changes and driving cause in Xiong'an, China: from dense Landsat time series images and synthetic analysis. Sci. Bull. 63 (11), 708–716.

Statistics, N.b.o., 2019. China Statistical Yearbook. Beijing: China Statistics Press.

Tao, S., Fang, J., Zhao, X., Zhao, S., Shen, H., Hu, H., Tang, Z., Wang, Z., Guo, Q., 2015. Rapid loss of lakes on the Mongolian Plateau. Proc Natl Acad Sci U S A 112 (7), 2281–2286.

Ukkola, A.M., De Kauwe, M.G., Roderick, M.L., Abramowitz, G., Pitman, A.J., 2020. Robust Future Changes in Meteorological Drought in CMIP6 Projections Despite Uncertainty in Precipitation. Geophys. Res. Lett. 47 (11).

Verpoorter, C., Kutser, T., Seekell, D.A., Tranvik, L.J., 2014. A global inventory of lakes based on high-resolution satellite imagery. Geophys. Res. Lett. 41 (18), 6396–6402.

Vörösmarty, C.J., McIntyre, P.B., Gessner, M.O., Dudgeon, D., Prusevich, A., Green, P., Glidden, S., Bunn, S.E., Sullivan, C.A., Liermann, C.R., Davies, P.M., 2010. Global threats to human water security and river biodiversity. Nature 467 (7315), 555–561.

Wang, L., Tian, F., Wang, Y., Wu, Z., Schurgers, G., Fensholt, R., 2018. Acceleration of global vegetation greenup from combined effects of climate change and human land management. Glob. Change Biol. 24 (11), 5484–5499.

Wang, X., Xiao, X., Zou, Z., Chen, B., Ma, J., Dong, J., Doughty, R.B., Zhong, Q., Qin, Y., Dai, S., Li, X., Zhao, B., Li, B., 2020a. Tracking annual changes of coastal tidal flats in China during 1986–2016 through analyses of Landsat images with Google Earth Engine. Remote Sens. Environ. 238, 110987.

Wang, X., Xiao, X., Zou, Z., Dong, J., Qin, Y., Doughty, R.B., Menarguez, M.A., Chen, B., Wang, J., Ye, H., Ma, J., Zhong, Q., Zhao, B., Li, B., 2020b. Gainers and losers of surface and terrestrial water resources in China during 1989–2016. Nat. Commun. 11 (1), 3471.

Wik, M., Varner, R.K., Anthony, K.W., MacIntyre, S., Bastviken, D., 2016. Climate-sensitive northern lakes and ponds are critical components of methane release. Nat. Geosci. 9 (2), 99–105.

Wulder, M.A., Coops, N.C., 2014. Make Earth observations open access. Nature 513 (7516), 30–31.

Wulder, M.A., Hilker, T., White, J.C., Coops, N.C., Masek, J.G., Pflugmacher, D., Crevier, Y., 2015. Virtual constellations for global terrestrial monitoring. Remote Sens. Environ. 170, 62–76.

Wulder, M.A., White, J.C., Loveland, T.R., Woodcock, C.E., Belward, A.S., Cohen, W.B., Fosnight, E.A., Shaw, J., Masek, J.G., Roy, D.P., 2016. The global Landsat archive: status, consolidation, and direction. Remote Sens. Environ. 185, 271–283.

Xie, C., Huang, X., Mu, H., Yin, W., 2017. Impacts of land-use changes on the lakes across the Yangtze Floodplain in China. Environ. Sci. Technol. 51 (7), 3669–3677.

Xin, Y., Lu, N., Jiang, H., Liu, Y., Yao, L., 2021. Performance of ERA5 reanalysis precipitation products in the Guangdong-Hong Kong-Macao greater Bay Area, China. J. Hydrol. 602, 126791.

Xu, L., Chen, N., Zhang, X., Chen, Z., 2019. Spatiotemporal Changes in China's Terrestrial Water Storage From GRACE Satellites and Its Possible Drivers. J. Geophys. Res.-Atmos. 124 (22), 11976–11993.

Xu, Y., Mo, X., Cai, Y., Li, X., 2005. Analysis on groundwater table drawdown by land use and the quest for sustainable water use in the Hebei Plain in China. Agric. Water Manag. 75 (1), 38–53.

Yamazaki, D., Trigg, M.A., Ikeshima, D., 2015. Development of a global similar to 90 m water body map using multi-temporal Landsat images. Remote Sens. Environ. 171, 337–351.

Yang, J., Dong, J., Xiao, X., Dai, J., Wu, C., Xia, J., Zhao, G., Zhao, M., Li, Z., Zhang, Y., Ge, Q., 2019. Divergent shifts in peak photosynthesis timing of temperate and alpine grasslands in China. Remote Sens. Environ. 233, 111395.

Yang, Z., Fang, C., Li, G., Mu, X., 2021. Integrating multiple semantics data to assess the dynamic change of urban green space in Beijing, China. Int. J. Appl. Earth Obs. Geoinf. 103, 102479.

You, N., Dong, J., 2020. Examining earliest identifiable timing of crops using all available Sentinel 1/2 imagery and Google Earth Engine. ISPRS J. Photogramm. Remote Sens. 161, 109–123.

Zhan, S., Song, C., Wang, J., Sheng, Y., Quan, J., 2019. A global assessment of terrestrial evapotranspiration increase due to surface water area change. Earth's Future 7 (3), 266–282.

Zhang, Y., Kong, D., Gan, R., Chiew, F.H.S., McVicar, T.R., Zhang, Q., et al., 2019b. Coupled estimation of 500 m and 8-day resolution global evapotranspiration and gross primary production in 2002–2017. Remote Sens. Environ. 222, 165–182.

Zhang, Y., Wang, Y., Niu, H., 2019c. Effects of temperature, precipitation and carbon dioxide concentrations on the requirements for crop irrigation water in China under future climate scenarios. Sci. Total Environ. 656, 373–387.

Zhang, G., Xie, H., Kang, S., Yi, D., Ackley, S.F., 2011. Monitoring lake level changes on the Tibetan Plateau using ICESat altimetry data (2003–2009). Remote Sens. Environ. 115 (7), 1733–1742.

Zhang, G., Yao, T., Piao, S., Bolch, T., Xie, H., Chen, D., Gao, Y., O'Reilly, C.M., Shum, C. K., Yang, K., Yi, S., Lei, Y., Wang, W., He, Y., Shang, K., Yang, X., Zhang, H., 2017. Extensive and drastically different alpine lake changes on Asia's high plateaus during the past four decades. Geophys. Res. Lett. 44 (1), 252–260.

Zhang, G., Yao, T., Chen, W., Zheng, G., Shum, C.K., Yang, K., Piao, S., Sheng, Y., Yi, S., Li, J., O'Reilly, C.M., Qi, S., Shen, S.S.P., Zhang, H., Jia, Y., 2019a. Regional differences of lake evolution across China during 1960s–2015 and its natural and anthropogenic causes. Remote Sens. Environ. 221, 386–404.

Zhang, G., Yao, T., Xie, H., Yang, K., Zhu, L., Shum, C.K., Bolch, T., Yi, S., Allen, S., Jiang, L., Chen, W., Ke, C., 2020. Response of Tibetan Plateau lakes to climate change: trends, patterns, and mechanisms. Earth Sci. Rev. 208, 103269.

Zhao, M., A, G., Zhang, J., Velicogna, I., Liang, C., Li, Z., 2020. Ecological restoration impact on total terrestrial water storage. Nat. Sustainability 4 (1), 56–62.

Zhao, G., Dong, J., Cui, Y., Liu, J., Zhai, J., He, T., Zhou, Y., Xiao, X., 2019. Evapotranspiration-dominated biogeophysical warming effect of urbanization in the Beijing-Tianjin-Hebei region, China. Clim. Dyn. 52 (1-2), 1231–1245.

Zhou, Y., Dong, J.W., Liu, J.Y., Metternicht, G., Shen, W., You, N.S., et al., 2019a. Are there sufficient landsat observations for retrospective and continuous monitoring of land cover changes in China? Remote Sens. 11 (15), 1808.

Zhou, Y., Dong, J., Xiao, X., Liu, R., Zou, Z., Zhao, G., Ge, Q., 2019b. Continuous monitoring of lake dynamics on the Mongolian Plateau using all available Landsat imagery and Google Earth Engine. Sci. Total Environ. 689, 366–380.

Zhu, Z., Woodcock, C.E., 2014. Automated cloud, cloud shadow, and snow detection in multitemporal Landsat data: an algorithm designed specifically for monitoring land cover change. Remote Sens. Environ. 152, 217–234.

Zhu, Z., Wulder, M.A., Roy, D.P., Woodcock, C.E., Hansen, M.C., Radeloff, V.C., Healey, S.P., Schaaf, C., Hostert, P., Strobl, P., Pekel, J.-F., Lymburner, L., Pahlevan, N., Scambos, T.A., 2019. Benefits of the free and open Landsat data policy. Remote Sens. Environ. 224, 382–385.

Zou, Z., Dong, J., Menarguez, M.A., Xiao, X., Qin, Y., Doughty, R.B., Hooker, K.V., David Hambright, K., 2017. Continued decrease of open surface water body area in Oklahoma during 1984–2015. Sci. Total Environ. 595, 451–460.

Zou, Z., Xiao, X., Dong, J., Qin, Y., Doughty, R.B., Menarguez, M.A., Zhang, G., Wang, J., 2018. Divergent trends of open-surface water body area in the contiguous United States from 1984 to 2016. PNAS 115 (15), 3810–3815.